Journal of Hazardous Materials 162 (2009) 254–263

Contents lists available at ScienceDirect

Journal of Hazardous Materials

journal homepage: www.elsevier.com/locate/jhazmat

# Chlorobenzene, chloroform, and carbon tetrachloride adsorption on undoped and metal-doped sol–gel substrates ($SiO_2$, $Ag/SiO_2$, $Cu/SiO_2$ and $Fe/SiO_2$)

M.A. Hernández[a,*], A.I. González[a], L. Corona[a], F. Hernández[a], F. Rojas[b], M. Asomoza[b], S. Solís[b], R. Portillo[c], M.A. Salgado[c]

[a] Postgrado de Ciencias Ambientales and Departamento de Investigación en Zeolitas, Instituto de Ciencias, Universidad Autónoma de Puebla, Edificio 76, Complejo de Ciencias, Ciudad Universitaria, CP 72570 Puebla, Mexico
[b] Departamento de Química, Universidad Autónoma Metropolitana-Iztapalapa, P.O. Box 55-534, D.F. México, Mexico
[c] Facultad de Ciencias Químicas, Universidad Autónoma de Puebla, Mexico

ARTICLE INFO

*Article history:*
Received 4 October 2007
Received in revised form 15 April 2008
Accepted 8 May 2008
Available online 16 May 2008

*Keywords:*
Adsorption of chlorinated compounds
Chlorobenzene adsorption
Chloroform adsorption
Carbon tetrachloride adsorption
Metal-doped silica substrates
Microporous and mesoporous sol–gel adsorbents
Isosteric heat of adsorption

ABSTRACT

Adsorption isotherms of chlorobenzene, chloroform and carbon tetrachloride vapors on undoped $SiO_2$, and metal-doped $Ag/SiO_2$, $Cu/SiO_2$ and $Fe/SiO_2$ substrates were measured in the temperature range of 398–593 K. These substrates were prepared from a typical sol–gel technique in the presence of metal dopants that rendered an assortment of microporous–mesoporous solids. The relevant characteristic of these materials was the different porosities and micropore to mesopore volume ratios that were displayed; this was due to the effect that the cationic metal valence exerts on the size of the sol–gel globules that compose the porous solid. The texture of these $SiO_2$ materials was analyzed by X-ray diffraction (XRD), FTIR, and diverse adsorption methods. The pore-size distributions of the adsorbents confirmed the existence of mesopores and supermicropores, while ultramicropores were absent. The Freundlich adsorption model approximately fitted the chlorinated compounds adsorption data on the silica substrates by reason of a heterogeneous energy distribution of adsorption sites. The intensity of the interaction between these organic vapors and the surface of the $SiO_2$ samples was analyzed through evaluation of the isosteric heat of adsorption and standard adsorption energy; from these last results it was evident that the presence of metal species within the silica structure greatly affected the values of both the amounts adsorbed as well as of the isosteric heats of adsorption.



## 1. Introduction

Chlorinated hydrocarbon compounds ($C_XH_YCl_Z$) such as chlorobenzene, chloroform, and carbon tetrachloride, can represent hazardous or harmful substances. The effective trapping of these compounds in the pores of mesoporous and microporous adsorbents represents a straightforward option to reduce the presence of these substances in the environment. The 2005 CERCLA Priority List of Hazardous Substances [1] ranks $CHCl_3$ as 11th, $CCl_4$ as 43rd, and $C_6H_5Cl$ as 108th in view of their known or suspected toxicities. $CCl_4$ inhalation can cause degeneration of liver and kidneys, chronic $CHCl_3$ exposure can induce severe liver damage and cardiac arrhythmia, and $C_6H_5Cl$ contact can be responsible of central nervous system ill-effects and renal degeneration.

The adsorption extent of volatile molecules on the surface of porous materials depends on the physicochemical characteristics of these molecules as well as on the chemical nature and textural properties of the adsorbent substrate such as pore size and number of interconnection paths between voids. If adsorption takes place inside micropores smaller than twice the diameter of the adsorbate molecule, the enhancement of the adsorption energy is caused by the overlapping of the potential fields emanating from both sides of the pore walls; i.e., a mechanism labeled as *micropore volume filling* arises [2]. Due to this enhanced adsorption attribute (in comparison to typical mesoporous adsorbents) many solids with pores of molecular dimensions (micropores) are often used as effective adsorbents in industrial applications.

Adsorption isotherm analysis has provided supporting evidence for the incidence of two main stages of micropore volume filling [3]: (a) a *primary* process involving enhanced adsorbent–adsorbate interactions in the so-called *ultramicropores* (i.e. voids smaller than 0.7 nm), and (b) a cooperative (*secondary*) process that can occur

* Corresponding author. Tel.: +52 2222 29 55 00x7270; fax: +52 2222 29 55 17.
*E-mail address:* mighern@siu.buap.mx (M.A. Hernández).

0304-3894/$ – see front matter © 2008 Elsevier B.V. All rights reserved.
doi:10.1016/j.jhazmat.2008.05.051

in *supermicropores* (i.e. *micropore* voids of sizes between 0.7 and 2.0 nm) by virtue of the cohesion forces developed between the adsorbed molecules that are being captured inside the micropore volume. The limiting width for primary micropore filling appears to be little more than two molecular diameters of the adsorptive molecule. Thus, the upper pore size limit for primary micropore filling by $N_2$ is ~0.7–0.8 nm (i.e. ultramicropores). In turn, the upper limit for secondary micropore filling depends on the adsorbate–adsorbate interactions and is probably in the region of five molecular diameters (~2 nm for $N_2$). Having these limits in mind, $N_2$ primary micropore filling usually finishes at relative pressures ($p/p^0$, where $p^0$ is the saturation vapor pressure of the adsorptive substance) well before 0.01 at which point supermicropore filling can already be taking place.

Several works dedicated to the above aspects were developed by diverse authors [4–7], particularly the adsorption of $N_2$ and $CO_2$ on microporous $SiO_2$ was investigated by Brinker et al. [8]. A few studies have been reported on the adsorption of butane and butene [9] on this type of solids. Limpo et al. [10] have characterized silica sol–gel materials synthesized from tetraethylorthosilicate and calcined at several temperatures. Raman et al. [11] have studied the porosity of silica solids. Hernández et al. [12,13] have pursued studies on the adsorption of hydrocarbons on microporous $SiO_2$. Meixner et al. [14] have investigated the adsorption of carbon tetrachloride, trimethylbenzene and perfluorotributylamine on microporous $SiO_2$. Furthermore, it is advisable to evaluate the mechanism of micropore volume filling at low pressures through the adsorption of different molecular probes [15].

Here, the results of a comparative study of this kind are reported for the adsorption of chlorobenzene, $C_6H_5Cl$; chloroform, $CHCl_3$; carbon tetrachloride, $CCl_4$) on a series of undoped ($SiO_2$) and metal-doped silica adsorbents ($Ag/SiO_2$, $Cu/SiO_2$, $Fe/SiO_2$) prepared by the sol–gel route. These substrates are endowed with micropores and mesopores. The corresponding adsorption isotherms are measured by gas chromatography measurements.

The present manuscript is organized as follows. Experimental details are given below; these include: synthesis of undoped and metal-doped $SiO_2$ sol–gel materials, information about the instruments employed for experimental characterization techniques and $C_XH_YCl_Z$ isothermal adsorption determination by gas chromatography retention time measurements. Several methods of analysis for the determination of some pore structural parameters are succinctly described. Finally, an evaluation of the characterization results in terms of the pore structure of the diverse $SiO_2$ substrates is presented.

## 2. Materials and methods

### 2.1. Materials

The adsorbents consisted of a series of undoped and metal-doped silica gels ($SiO_2$, $Ag/SiO_2$, $Cu/SiO_2$ and $Fe/SiO_2$) prepared by the sol–gel technique. Tetraethylorthosilicate (TEOS, Aldrich 98 wt.%) was chosen as the key reactant for the sol–gel synthesis of $SiO_2$ porous substrates. Ethanol (J.T. Baker 99.9%, v/v) was the liquid medium in which the sol–gel reactions took place. $AgNO_3$ (J.T. Baker 99.7 wt.%,), $Cu(NO_3)_2{\cdot}2.5H_2O$ (J.T. Baker 98 wt.%) and $Fe(NO_3)_3{\cdot}9H_2O$ (J.T. Baker 98 wt.%) salts constituted the metal dopant sources. High-purity chlorobenzene (Aldrich 99.99 wt.%) chloroform (Aldrich 99.9 wt.%), and carbon tetrachloride (Aldrich 99.9 wt.%) were used as adsorptives. All chemicals were employed as supplied without further purification. High-purity helium and nitrogen gases (99.999%, LINDE) were used for GC and sorption measurements.

### 2.2. Syntheses of undoped and metal-doped $SiO_2$ microporous–mesoporous samples

Porous silica monoliths were synthesized from reactant mixtures consisting of TEOS dissolved in ethanol; this solution was subsequently mixed with deionized water according to 1 TEOS:4 EtOH:2.5 $H_2O$ molar ratios. The reactant mixture was prepared inside a cylindrical glass column that was maintained at 303 K. The resulting sol was kept undisturbed in the original column until gelation eventually occurred (i.e. a period of several months was usually required). The ensuing gel was then dried in situ at 373 K for 48 h so that a cylindrical monolith of microporous silica was finally attained. The specimen prepared this way was labelled as $SiO_2$. In turn, the $Ag/SiO_2$, $Cu/SiO_2$, and $Fe/SiO_2$ substrates were synthesized in the following way. The required amount of $AgNO_3$, $Cu(NO_3)_2$, or $Fe(NO_3)_3$ in order to reach a $SiO_2$ substrate containing 0.15 wt.% Ag, Cu, or Fe, respectively, was added to the volume of water involved in the $SiO_2$ sol synthesis; otherwise, the conditions selected for the preparation of these latter specimens were the same as those related to the production of metal-free $SiO_2$.

### 2.3. Measurement techniques

X-ray diffraction (XRD) patterns were determined by means of a Siemens D-500 diffractometer employing a nickel-filtered Cu Kα radiation in the $2\theta$ diffraction angle range extending from 5 to 60°, intensity values were read at $\Delta(2\theta)$ intervals of 0.02° employing a step time of 1.2 s. FTIR analyses were carried out in a Bruker Vector 22 spectrometer.

$N_2$ adsorption isotherms were measured at the boiling point of liquid $N_2$ (76 K at the 2240-m altitude of Puebla City, Mexico) in an automatic volumetric adsorption system (Quantachrome Autosorb-1LC). $N_2$ adsorption isotherms were determined in the interval of relative pressures, $p/p^0$, extending from $10^{-5}$ to 0.995. The saturation pressure, $p^0$, was continuously registered in the course of the adsorption–desorption measurements. Powder particle sizes corresponding to mesh 60–80 were sampled from all

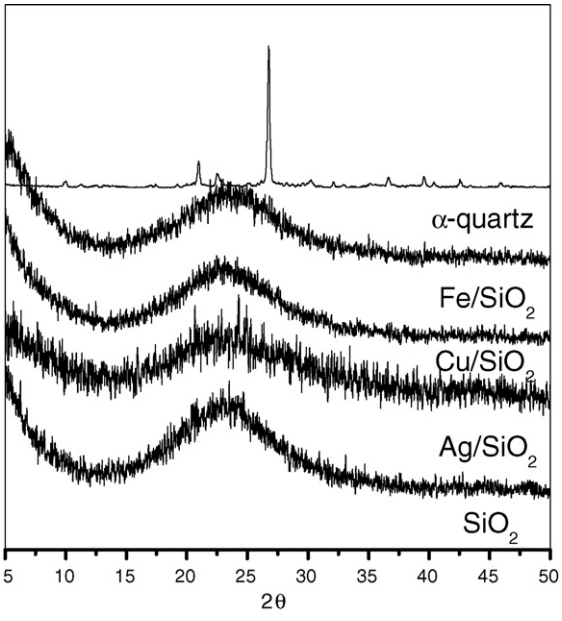


**Fig. 1.** XRD patterns of undoped and metal-doped $SiO_2$ sol–gel substrates. An α-quartz crystalline diffraction pattern is included for comparison.

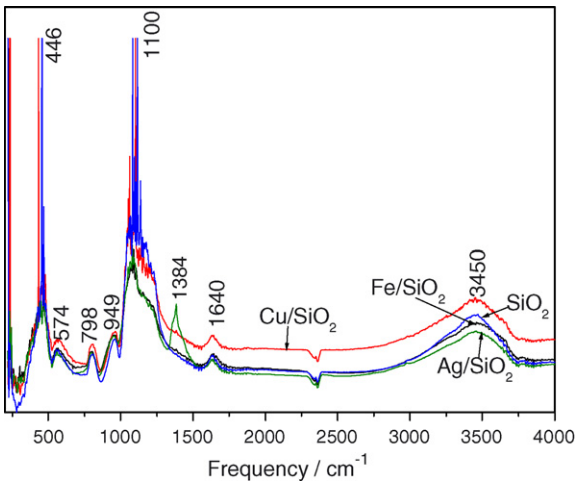


**Fig. 2.** FTIR spectra of undoped and metal-doped $SiO_2$ sol–gel substrates.

specimens under analysis. Prior to the sorption experiments, every sample was outgassed at 623 K during 20 h at a pressure lesser than $10^{-6}$ mbar. The BET and $\alpha_S$ [16] surface areas of the $SiO_2$ substrata under study were evaluated from the analysis of $N_2$ adsorption data. The total pore volume, $V_{\sum}$, was estimated through the Gurvitsch rule on the basis of the volume adsorbed at the relative pressure $p/p^0 \sim 0.95$ and calculated as volume of liquid. Information about the pore size distributions (PSD) of the $SiO_2$ under study was obtained from both the non-local density functional theory (NLDFT) [17,18] approach. The microporosity inherent to the $SiO_2$ samples was studied by way of the $\alpha_S$-plot method ($\alpha_S$ is Sing's standard reduced parameter defined as the ratio of the volume adsorbed at the current $p/p^0$ to the volume adsorbed at $p/p^0 = 0.4$); the non-porous silica reference material employed to construct the $\alpha_S$-plot was that of Gregg and Sing [16].

### 2.4. $C_XH_YCl_Z$ adsorption

Chromatographic adsorption measurements of $C_6H_5Cl$, $CHCl_3$, and $CCl_4$ were carried out in a GC-14A Shimadzu gas chromatograph equipped with a thermal conductivity detector. The chromatographic columns (i.d. = 5 mm, length = 50 cm) were made of glass and packed with 60–80 mesh silica grains. Adsorbate pulses of different intensities were injected into the packed silica columns that were kept at the chosen temperature, and the elution chromatogram of each pulse was registered. Prior to the adsorption experiment, adsorbents were pre-treated in situ under a He flow at 573 K for 8 h. Each chlorinated compound was injected separately into the appropriate chromatographic column in order to measure the corresponding chromatogram.

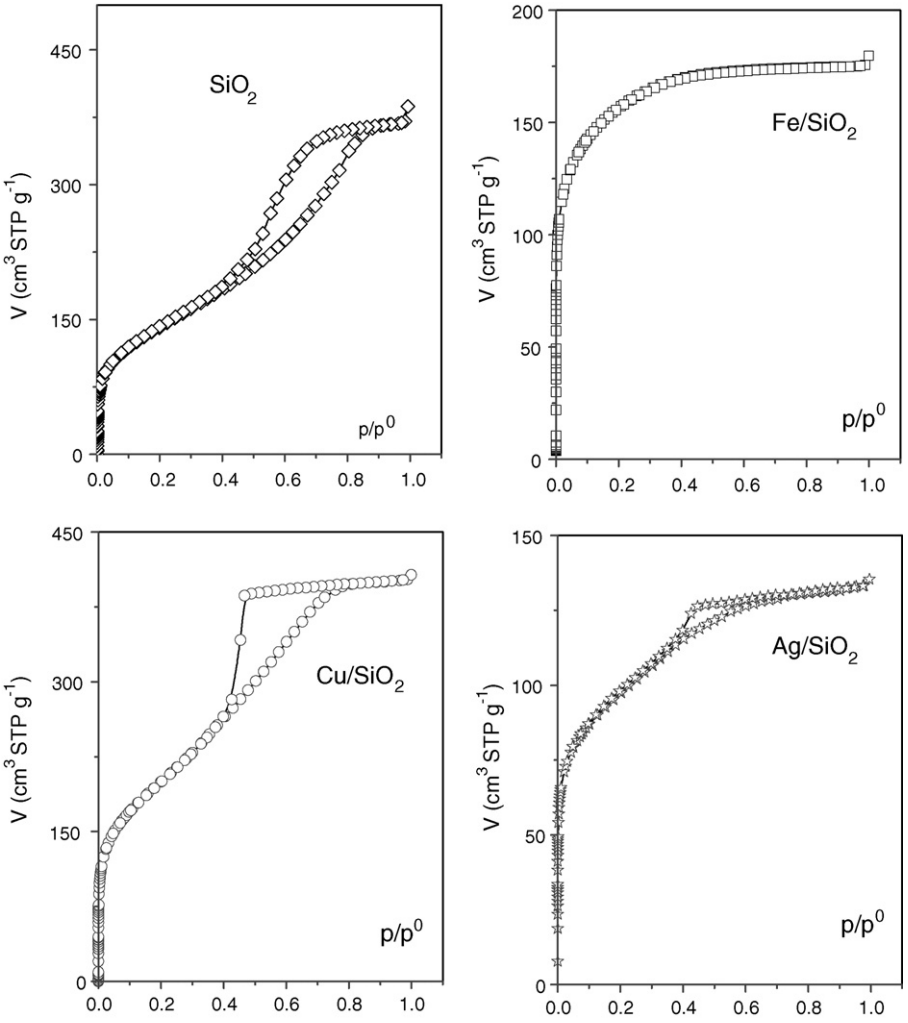


**Fig. 3.** Nitrogen adsorption isotherms on undoped and metal-doped $SiO_2$ sol–gel substrates at 76 K.

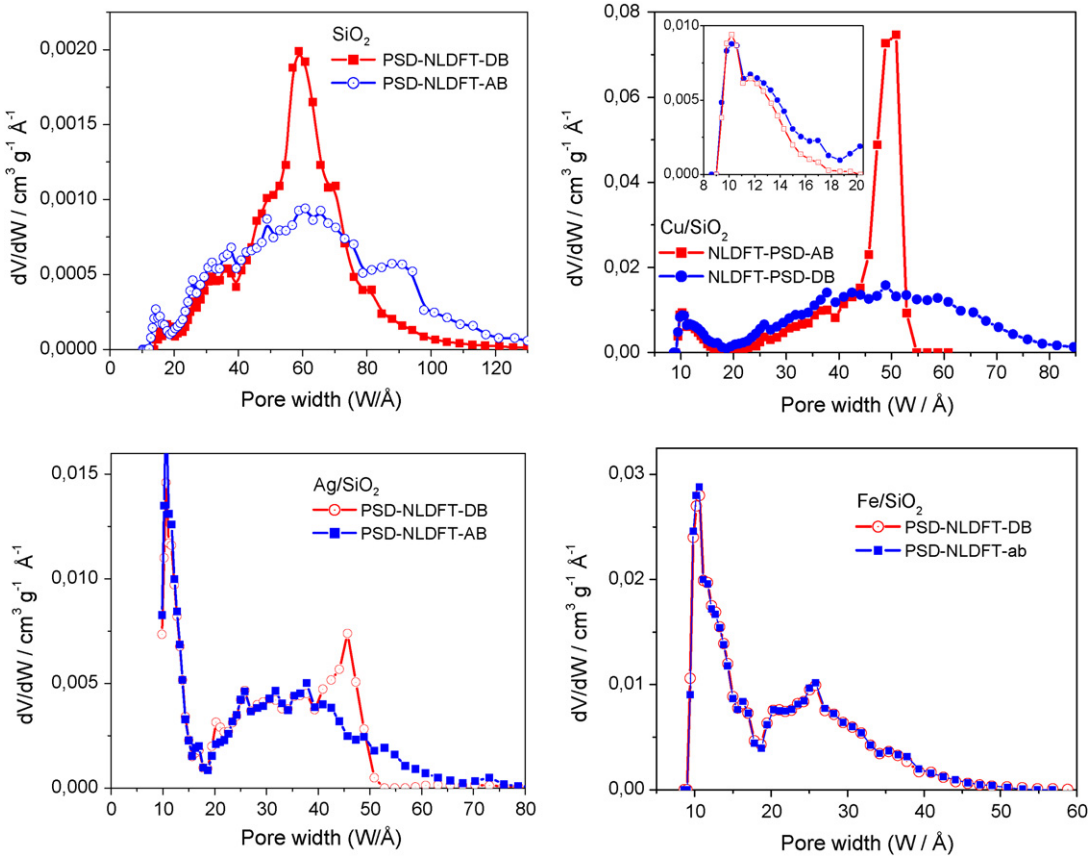


**Fig. 4.** Pore size distributions calculated through the NLDFT approach from adsorption boundary (AB) and desorption boundary (DB) $N_2$ isotherms at 76 K on undoped and metal doped $SiO_2$ substrates. The inset in Fig. 3b is an enlargement of the supermicropore region of sample $Cu/SiO_2$.

*2.4.1. Calculation methods*

$C_6H_5Cl$, $CHCl_3$, and $CCl_4$ adsorption data on undoped and doped $SiO_2$ adsorbents were fitted to the standard Freundlich adsorption equation through linear regression. The Freundlich adsorption equation [19] can be written as

$$a = K_F p^{1/n} \quad (\text{where } n > 1) \tag{1}$$

where $a$ is the amount adsorbed (mmol $g^{-1}$) at pressure $p$, $K_F$ the Freundlich adsorption constant, and $1/n$ is an exponential factor.

Standard adsorption energies ($-\Delta U_0$) can be found from the temperature dependence of Henry constants $K_H$ (at low pressures $K_H \approx K_F$), a relationship that is assumed to be consistent with a traditional van't Hoff form:

$$\frac{\partial \ln K_H}{\partial T} = \frac{\Delta U_0}{RT^2}; \quad K_H = K_0 \exp\left(\frac{-\Delta U_0}{RT}\right) \tag{2}$$

where $\Delta U_0 = \Delta H_0 + RT$; $\Delta H_0$ is the standard adsorption enthalpy, $R$ the universal gas constant, and $K_0$ is van't Hoff's pre-exponential factor. The isosteric heat of adsorption of each $SiO_2$ sample was calculated from the Clausius–Clapeyron equation [20]:

$$-q_{st} = R\left[\frac{\partial \ln p}{\partial(1/T)}\right]_a \tag{3}$$

**Table 2**
Pore mode widths[a] ($W$) on undoped and metal-doped $SiO_2$ samples as calculated through the NLDFT method of analysis from the ascending boundary (AB) isotherm

| Adsorbent | $W$ (Å) |
|---|---|
| $SiO_2$ | 60.4 |
| $Cu/SiO_2$ | 9.9, 48.7 |
| $Fe/SiO_2$ | 10.5, 25.7 |
| $Ag/SiO_2$ | 10.6, 37.7 |

[a] The existence of two values in a given cell indicates a bimodal PSD.

**Table 1**
Pore structure parameters of undoped and metal-doped $SiO_2$ sol–gel samples as calculated from $N_2$ adsorption data

| Adsorbent | $A_{BET}$ ($m^2\ g^{-1}$) | $A_{\alpha_S}$ ($m^2\ g^{-1}$) | $V_{\sum}$ ($cm^3\ g^{-1}$) | $\varepsilon$ | $W_0$ ($cm^3\ g^{-1}$) | $W_0/V_{\sum}$ | $4V_{\sum}/A_{BET}$ (Å) |
|---|---|---|---|---|---|---|---|
| $SiO_2$ | 511 | 560 | 0.564 | 0.554 | 0.011 | 0.019 | 44.2 |
| $Ag/SiO_2$ | 345 | 253 | 0.204 | 0.310 | 0.062 | 0.304 | 23.7 |
| $Fe/SiO_2$[a] | 553 | 381 | 0.269 | 0.372 | 0.126 | 0.468 | 19.5 |
| $Cu/SiO_2$ | 718 | 604 | 0.617 | 0.576 | 0.042 | 0.068 | 34.4 |

$A_{BET}$, is the BET surface area, $A_{\alpha_S}$ is the external surface area calculated from the $\alpha_S$ plot, $V_{\sum}$ is the total pore volume determined at $p/p^0 \sim 0.95$, $\varepsilon$ is the porosity, $W_0$ is the micropore volume calculated from the $\alpha_S$ plot, and $W_0/V_{\sum}$ is the micropore to mesopore volume ratio.

[a] The micropore volume of the $Fe/SiO_2$ was obtained from the NLDFT-PSD.

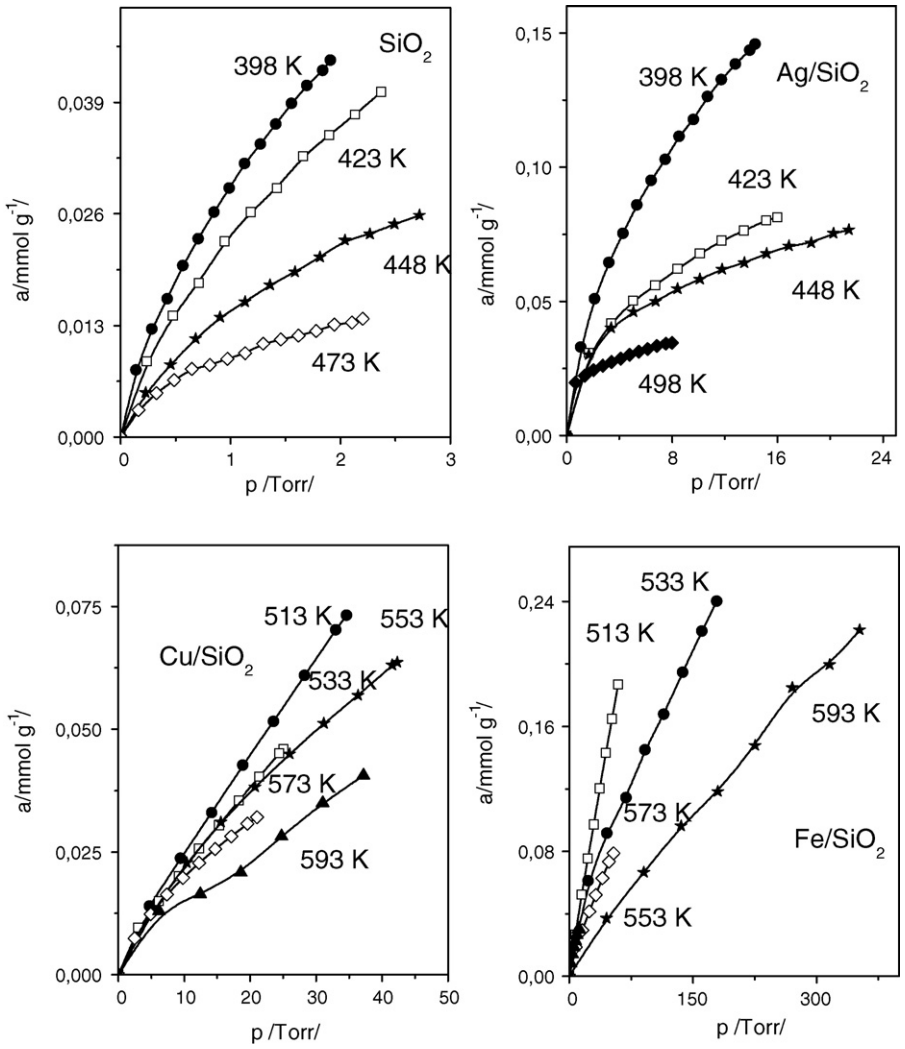


**Fig. 5.** Adsorption isotherms of $CHCl_3$ on undoped and metal-doped $SiO_2$ sol–gel substrates.

where $p$ is the equilibrium pressure for reaching a particular surface coverage $a$ and $T$ is the temperature.

## 3. Results and discussion

### 3.1. Characterization of $SiO_2$ substrates

XRD analysis of $SiO_2$ adsorbents (see Fig. 1) rendered typical patterns related to amorphous $SiO_2$ materials. The amorphous $SiO_2$ structure of the synthesized $SiO_2$ adsorbents was confirmed by the wide diffraction pattern that was displayed by these materials; in contrast the crystalline lattice of an α-quartz $SiO_2$ material depicted a succession of sharp peaks.

### 3.2. FTIR of $SiO_2$ substrates

The FTIR spectra of the pure and metal-doped $SiO_2$ adsorbents (Fig. 2) show a rather broad band centered at about 3450 $cm^{-1}$; this signal is due to adsorbed or hydrogen-bonded water molecules [21]. The peak appearing at 1640 $cm^{-1}$ is due to flexion vibrations of the O–H groups of water molecules. The bands existing at 1100, 798, and 446 $cm^{-1}$ correspond to the stretching vibrations of the mesoporous framework (Si–O–Si) bridges. These three bands represent the symmetric and asymmetric stretching vibration modes of the Si–O–Si bonds as well as the bending vibrations of the silica network structure. The signal located at 949 $cm^{-1}$ can be assigned to the stretching vibrations of the Si–OH silanol groups. Finally, the small band found at approximately 1384 $cm^{-1}$ has been suggested to reflect the Ag–O bond vibration [22].

From the above information about the presence of certain surface groups, it is likely that the adsorption of $C_6H_5Cl$, $CHCl_3$, and $CCl_4$ molecules depends to some extent on the dipolar moments (1.01 D for $CHCl_3$, 0 D for $CCl_4$, and 1.6 D for $C_6H_5Cl$). Due to the existence of silanol (i.e. oxygenated) groups on the surface of the silica adsorbents, it is then possible that the adsorption of chlorinated compounds onto the silica surface is somewhat influenced by the formation of weak hydrogen bonds between the chlorine atoms of the chlorinated molecules and the hydrogen atoms of surface silanol groups.

### 3.3. $N_2$ sorption isotherms

Nitrogen sorption isotherms for the set of the $SiO_2$ precursory and doped (Ag, Fe and Cu) $SiO_2$ samples are shown in Fig. 3 (relative pressure $p/p^0$ vs. adsorbed $N_2$ volume in $cm^3$ STP per gram

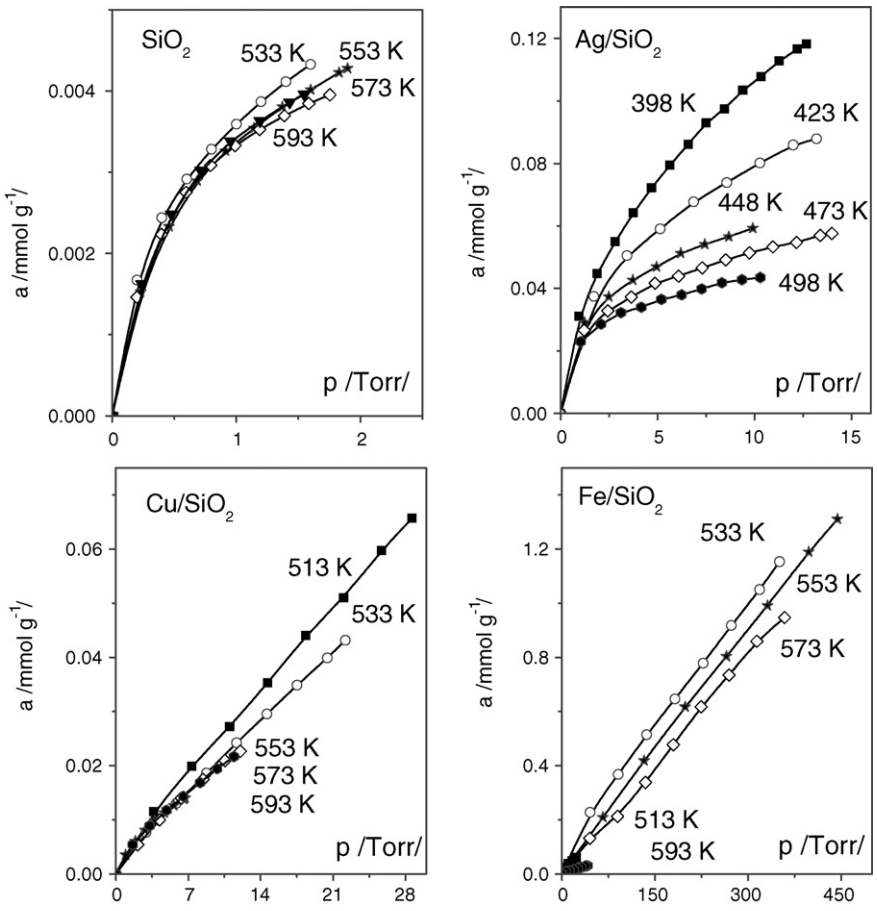


**Fig. 6.** Adsorption isotherms of $CCl_4$ on undoped and metal-doped $SiO_2$ sol–gel substrates.

of adsorbent). This figure portrays the particularities of each one of these $N_2$ isotherm shapes. The $SiO_2$, and $Cu/SiO_2$, and $Ag/SiO_2$ substrata render IUPAC Type IV isotherms, while an IUPAC Type I isotherm is proper of the $Fe/SiO_2$ specimen.

### *3.4. Pore-size distributions of undoped and metal-doped $SiO_2$ substrates calculated by the NLDFT approach*

The distributions of pore sizes in the $SiO_2$ adsorbents were approximated by the NLDFT approach [23]. Actually, this proposal is only exactly applicable to pores of single, idealized shapes, such as cylindrical, spherical, or slit-like voids. The NLDFT treatment takes into account all kind of solid–fluid and fluid–fluid interactions according to the pore geometry; the ultimate goal is to find the minimum of the so called grand potential functional for a fluid confined in a pore at a given chemical potential and temperature. This condition allows to find the liquid–vapor meniscus shape and the pressure at which a vapor–liquid transition is occurring; in other words, a theoretical isotherm can be obtained for a given pore of a given shape and size. Having a set of isotherms for pores of the same shape but of different size allow the fitting of the experimental isotherm by the weighted superposition of the model isotherms. The weighing factors then lead to the determination of the PSD.

The pores of the undoped and metal-doped $SiO_2$ materials have no idealized shapes but correspond to voids between packed globules of varied sizes. The presence of polydisperse globules is proper of the sol–gel route. In our case, there exist two kinds of pores: *throats* (windows) and *cavities* [24]; each cavity is surrounded by a number of throats depending on the number of nearest neighbours that each globule has. When a condensing vapor surrounds the pores, capillary condensation first occurs in throats, i.e. around the saddle points existing between two contiguous spheres; afterward, condensation takes place in the cavities either by a vapor–liquid transition that occurs inside or by the advance of menisci that proceed from the surrounding throats.

In the present work, one can approximately assume that pore throats are in control of both capillary condensation and evaporation processes and that an elementary shape for them can be thought as short tubular (cylindrical) passages that surround spheroidal cavities. Therefore, by applying the NLDFT approach to our $SiO_2$ adsorbents, one could acquire a semiquantitative idea about the real pore sizes. Fig. 4 depicts the PSD curves obtained from the adsorption boundary (AB) and desorption boundary (DB) isotherms that delimit the sorption hysteresis loops of the diverse substrates.

The appearances of the $N_2$ sorption isotherms of $SiO_2$ undoped and metal-doped substrates primarily suggest pore structures consisting of either solely micropores ($Fe/SiO_2$) or purely mesopores ($SiO_2$, $Cu/SiO_2$, $Ag/SiO_2$); in reality, most of these samples consist of a combination of micropores and mesopores, as is evident from the PSD results obtained from the NLDFT approach. The pores in these substrates appear as voids between globules; the size of these globules has been largely determined by the electrovalence of the metallic dopant species; the largest the electrovalence of the ionic species the smaller the size of the resultant sol–gel globules and, therefore, of the pore sizes between these grains. While the undoped $SiO_2$ substrate can be classified as mostly mesoporous by virtue of the associated Type IV isotherm and Type H2 hysteresis

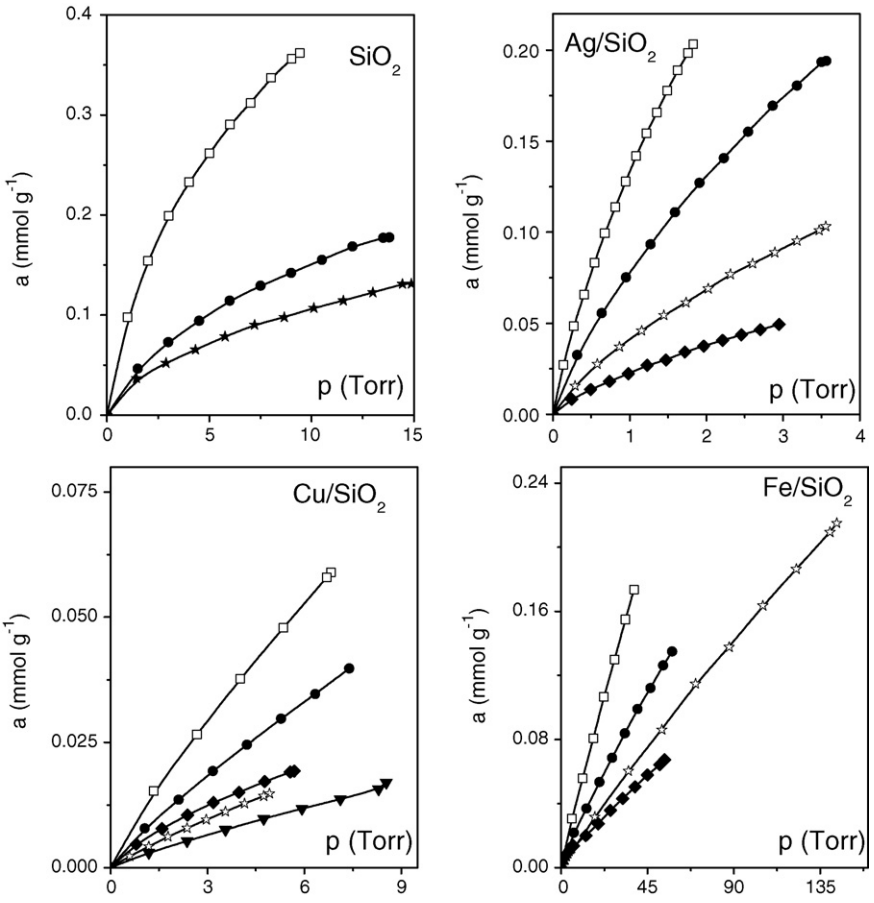


**Fig. 7.** Adsorption isotherms of $C_6H_5Cl$ on undoped and metal-doped $SiO_2$ sol–gel substrates.

loop, the remaining doped structures involve different micropore to mesopore content ratios.

Table 1 shows values of some important textural parameters obtained from the analysis of the $N_2$ sorption isotherms, such as surface areas total pore volumes, $V_{\sum}$, calculated according to the Gurvitsch rule [16] (applied at $p/p^0 = 0.95$). The micropore uptake capacities for each adsorbent and the ratios of the micropore-filling capacity to the total pore volume, $W_0/V_{\sum}$, are also included in Table 1. The PSD calculations were performed from the adsorption boundary (AB) and desorption boundary (DB) branches of the $N_2$ isotherms by using the NLDFT cylindrical pore model. The NLDFT approach can discern between supermicropores and mesopores, Fig. 4. The NLDFT results suggest that the dopant metals that are incorporated into the $SiO_2$ samples favor the formation of narrower pores if compared to those of the undoped silica substrate. Table 2 lists the pore size modes determined from the PSD proceeding from the AB isotherm. Each PSD case requires clarification in order to visualize the characteristics of the diverse pore structures assumed by the $SiO_2$ metal-doped and undoped adsorbents.

The pore size of the $SiO_2$ materials should be linked to the particle size of these substrates. For $SiO_2$ the average pore diameter $d_p$ calculated from the formula $d_p = 4V_{\sum}/A_{BET}$ renders 4.42 nm (see Table 1), while for $Ag/SiO_2$, $Cu/SiO_2$ and $Fe/SiO_2$ this $d_p$ value becomes 2.37, 3.44, and 1.95 nm, respectively. On the basis of elementary concepts about the stability of colloidal dispersions, it would be expected the undoped silica substrate to be the adsorbent with the largest particles, followed (in a decreasing order) by $Ag/SiO_2$, $Cu/SiO_2$ and $Fe/SiO_2$; this sequence is actually in accordance with the Schulze-Hardy rule [25] stating that the critical coagulation concentration for a lyophobic sol is extremely sensitive to the valence of the counter-ions (higher valence means a lower critical coagulation concentration). The Schulze-Hardy cation concentration required to provoke the flocculation of colloidal dispersions approximately follows a $1/z^2$ molar ratio sequence, i.e. 1:1/4:1/9 for monovalent, divalent and trivalent ions, respectively. With the exception of the $Cu/SiO_2$ specimen the average pore size resulted as predicted by the above rule.

Interesting textural characteristics of the $SiO_2$ substrates can be inferred as follows from the diverse isotherm and PSD shapes:

- The porosity figures, $\varepsilon$, listed in Table 1 indicate adsorbents endowed with fair amounts of total pore volumes in order to catch chlorinated vapors. In fact, typical porous silica adsorbents correspond to microporous–mesoporous substrates with porosity values ranging between 0.39 and 0.45 [13]; the $\varepsilon$, values of the doped and undoped silica samples thus allow to have enough room for the storage of chlorinated compounds. Highly porous silica corresponds to aerogel structures with porosities going up to more than 0.9 [26]; however, the handling and brittleness of these porous systems is troublesome if compared to xerogel substrates in the form of monoliths or granular solids.
- The $SiO_2$ and $Cu/SiO_2$ materials are mostly mesoporous structures; the micropore volumes of these substrates calculated from the PSD-NLDFT treatment accounts for only 0.011 and 0.042 $cm^3\,g^{-1}$ of micropore volume (the smallest values of all), respectively. Additionally, the total pore volumes of these materials are the highest of all. The isotherm of the $Cu/SiO_2$

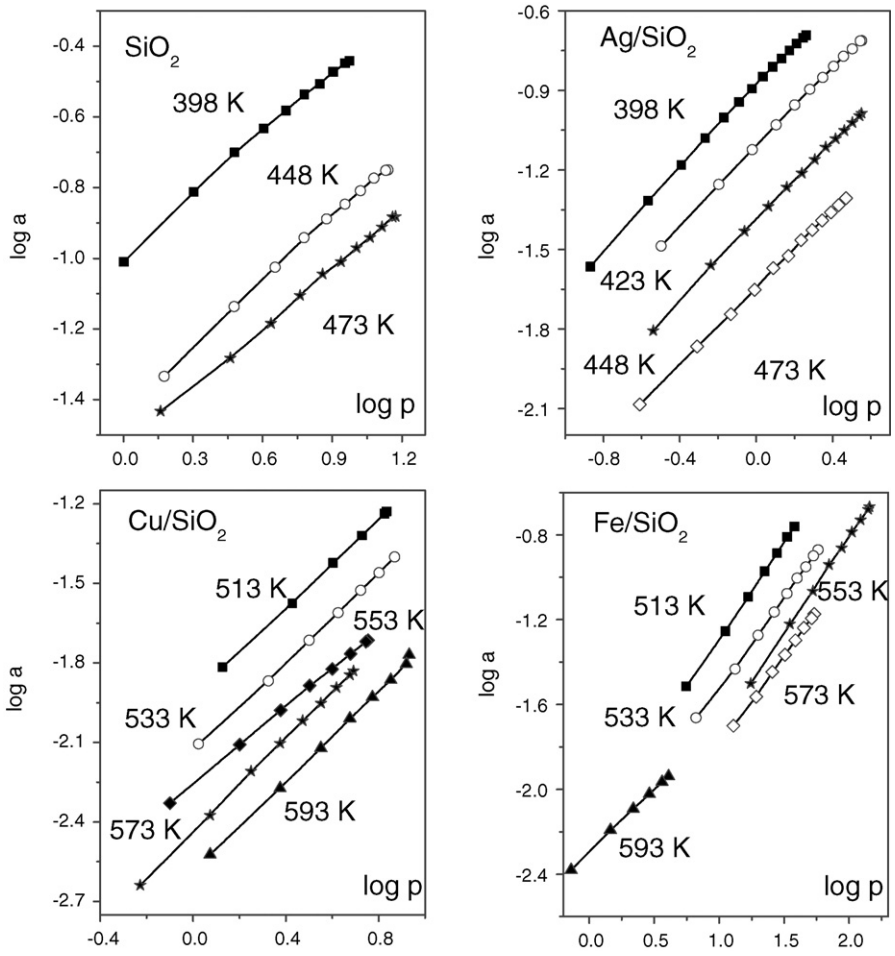


**Fig. 8.** Freundlich plots for the adsorption of $C_6H_5Cl$ on undoped and metal-doped $SiO_2$ sol–gel substrates at different temperatures.

sample indicates a vapor percolation phenomenon at a certain relative pressure range (i.e. 0.42–0.46) which is indicative of the sudden creation (and ulterior abrupt escape) of bubbles in the interior of the pores containing condensate (i.e. a cavitation phenomenon [27] is taking place). This cavitation phenomenon is somewhat less intense in the $SiO_2$ sample. The BET area of the $Cu/SiO_2$ specimen accounts for 718 $m^2\,g^{-1}$, while the cumulative surface area of supermicropores of sizes 9–19 Å is equivalent

**Table 3**
Freundlich parameters for adsorption of $C_6H_5Cl$, $CHCl_3$ and $CCl_4$ on $SiO_2$ sol–gel substrates

| Adsorbent | $T$ (K) | $K_{FC_6H_5Cl}$ ($\times 10^3$ mmol $g^{-1}$ $Torr^{-1}$) | $n_{C_6H_5Cl}$ | $K_{FCHCl_3}$ ($\times 10^3$ mmol $g^{-1}$ $Torr^{-1}$) | $n_{CHCl_3}$ | $K_{FCCl_4}$ ($\times 10^3$ mmol $g^{-1}$ $Torr^{-1}$) | $n_{CCl_4}$ |
|---|---|---|---|---|---|---|---|
| $SiO_2$ | 398 | 101.7 | 1.73 | 28.9 | 1.50 | 29.0 | 1.60 |
| | 423 | – | – | 23.0 | 1.51 | 22.5 | 1.54 |
| | 448 | 37.35 | 1.65 | 14.2 | 1.54 | 12.4 | 1.59 |
| | 473 | 29.61 | 1.80 | 9.224 | 1.86 | 7.30 | 1.70 |
| $Ag/SiO_2$ | 398 | 131.3 | 1.30 | 32.7 | 1.76 | 32.4 | 1.94 |
| | 423 | 77.45 | 1.35 | – | – | 29.9 | 2.37 |
| | 448 | 40.69 | 1.35 | 24.7 | 2.30 | 27.2 | 2.93 |
| | 473 | 22.77 | 1.38 | 25.4 | 2.77 | 24.9 | 3.15 |
| | 498 | – | – | 20.8 | 4.20 | 23.1 | 3.61 |
| $Cu/SiO_2$ | 513 | 11.91 | 1.20 | 3.70 | 1.19 | 3.68 | 1.17 |
| | 533 | 7.38 | 1.19 | 3.91 | 1.32 | 2.95 | 1.16 |
| | 553 | 3.66 | 1.14 | 3.84 | 1.33 | 3.83 | 1.44 |
| | 573 | 5.58 | 1.39 | 4.17 | 1.48 | 2.96 | 1.20 |
| | 593 | 2.55 | 1.16 | 3.52 | 1.53 | 3.82 | 1.41 |
| $Fe/SiO_2$ | 513 | 6.31 | 1.10 | 7.10 | 1.49 | 10.3 | 1.77 |
| | 533 | 4.17 | 1.17 | 4.17 | 1.07 | 10.3 | 1.25 |
| | 553 | 2.35 | 1.10 | 1.29 | 1.14 | 3.75 | 1.04 |
| | 573 | 2.23 | 1.17 | 3.61 | 1.30 | 2.73 | 1.01 |
| | 593 | 5.08 | 1.70 | 5.31 | 1.39 | 2.34 | 1.50 |

**Table 4**
Standard adsorption energies ($-\Delta U$, kJ mol$^{-1}$) of $C_6H_5Cl$, $CHCl_3$ and $CCl_4$ on $SiO_2$, $Ag/SiO_2$, $Cu/SiO_2$, and $Fe/SiO_2$ substrates

| Adsorbent/Adsorbate | $C_6H_5Cl$ | $CHCl_3$ | $CCl_4$ |
|---|---|---|---|
| $SiO_2$ | 26.46 | 24.28 | 29.34 |
| $Ag/SiO_2$ | 36.83 | 6.81 | 5.66 |
| $Cu/SiO_2$ | 42.70 | 0.28 | −0.79 |
| $Fe/SiO_2$ | 45.36 | 100.22 | 53.22 |

to 141 m$^2$ g$^{-1}$. The difference between the last two areas, i.e. 577 m$^2$ g$^{-1}$, can be assumed as the area of the mesopores existing in this sample. The $\alpha_S$ area proceeding from the corresponding plot corresponds to 604 m$^2$ g$^{-1}$ (Table 1), which is roughly the mesoporous contribution to the total surface area of the $Cu/SiO_2$ sample. The NLDFT-PSD plot of sample $Cu/SiO_2$ indicates micropores of sizes between 9 and 19 Å; these voids correspond to supermicropores (i.e. hollows in the range 7–20 Å [28]) and are recognized to be filled with $N_2$ at $p/p^0$ values below 0.01.

- The $Ag/SiO_2$ and $Fe/SiO_2$ have more definite contributions of micropores in their structures; these micropores coexist with mesopores according to different volumetric ratios, i.e. 0.304 and 0.468, respectively. The total pore volumes of these two samples account for the smallest values of the adsorbent series. The $Ag/SiO_2$ substrate appears to be microporous but there still exists a certain mesopore contribution; it is for this reason that a narrow hysteresis loop [29] appears at $p/p^0 \in [0.4,0.6]$.

The shape of the $N_2$ sorption isotherm related to the $Fe/SiO_2$ material is IUPAC Type I; nevertheless this isotherm is the result of a combination between supermicropores and small mesopores. The $Fe/SiO_2$ sample possesses equivalent volumes of micropores and mesopores: the NLDFT-PSD-DB result accounts for 12.6 mm$^3$ g$^{-1}$ of micropores having sizes in the range 9–19 Å, while 12.9 mm$^3$ g$^{-1}$ is related to mesopores of sizes 20–60 Å.

### 3.5. $C_XH_YCl_Z$ adsorption

Adsorption isotherms of $C_6H_5Cl$, $CHCl_3$, and $CCl_4$ measured at different temperatures on the different $SiO_2$ adsorbents are shown in Figs. 5–7. For all adsorptives, the linearity of the graph log $a$ versus log $p$ represents an acceptable indicator of the applicability of the Freundlich equation. With the exception of $CHCl_3$ adsorbed at 473 K on $SiO_2$, $Ag/SiO_2$ and $Cu/SiO_2$ as well as for $CCl_4$ adsorption at 513 and 593 K on $Fe/SiO_2$, the rest of the adsorption systems render good linear fittings to the Freundlich equation; Fig. 8 illustrates, for the case of $C_6H_5Cl$ adsorption, the quality of this Freundlich linear fitting.

The adsorption isotherms of chlorinated compounds on $SiO_2$ adsorbents exhibit a Type I shape therefore reflecting a relatively strong interaction between the surface of the adsorbents and the chlorinated molecules. The Freundlich parameters, $K_F$ and $n$, for the adsorption of chlorinated compounds on undoped and metal-doped $SiO_2$ adsorbents are presented in Table 3. The Freundlich exponents, $1/n$, show a temperature dependence for all the adsorption systems. For all adsorptives, the adsorption data could not be fitted to the Langmuir adsorption model, thus indicating a relatively broad (inhomogeneous) energy distribution of adsorption sites. This could be caused by the fact that the chlorinated adsorptive molecules have different characteristics (size, molecular mass, volume, and even dipole moments). The obtained values of the standard adsorption energies ($-\Delta U_0$) of $C_6H_5Cl$, $CHCl_3$, and $CCl_4$ on $SiO_2$, $Ag/SiO_2$, $Cu/SiO_2$ and $Fe/SiO_2$ are reported in Table 4, the ($-\Delta U_0$) magnitudes show the following sequence: ($-\Delta U_{0,C_6H_5Cl}$): $Fe/SiO_2 > Cu/SiO_2 > Ag/SiO_2 > SiO_2$; ($-\Delta U_{0,CHCl_3}$): $Fe/SiO_2 > SiO_2 > Ag/SiO_2 > Cu/SiO_2$ and ($-\Delta U_{0,CCl_4}$): $Fe/SiO_2 > SiO_2 > Ag/SiO_2 > Cu/SiO_2$.

#### 3.5.1. Isosteric heats of adsorption ($q_{st}$, kJ mol$^{-1}$)

Isosteric heats of adsorption are usually determined at low concentrations of the adsorbed molecules; under this circumstance the adsorbate–adsorbate interactions can be neglected in favor of the adsorbate–adsorbent interactions. The behavior of the isosteric heat of adsorption of the chlorinated compounds on the $SiO_2$ adsorbents is shown in Fig. 9. For each adsorptive, the $q_{st}$ values observe

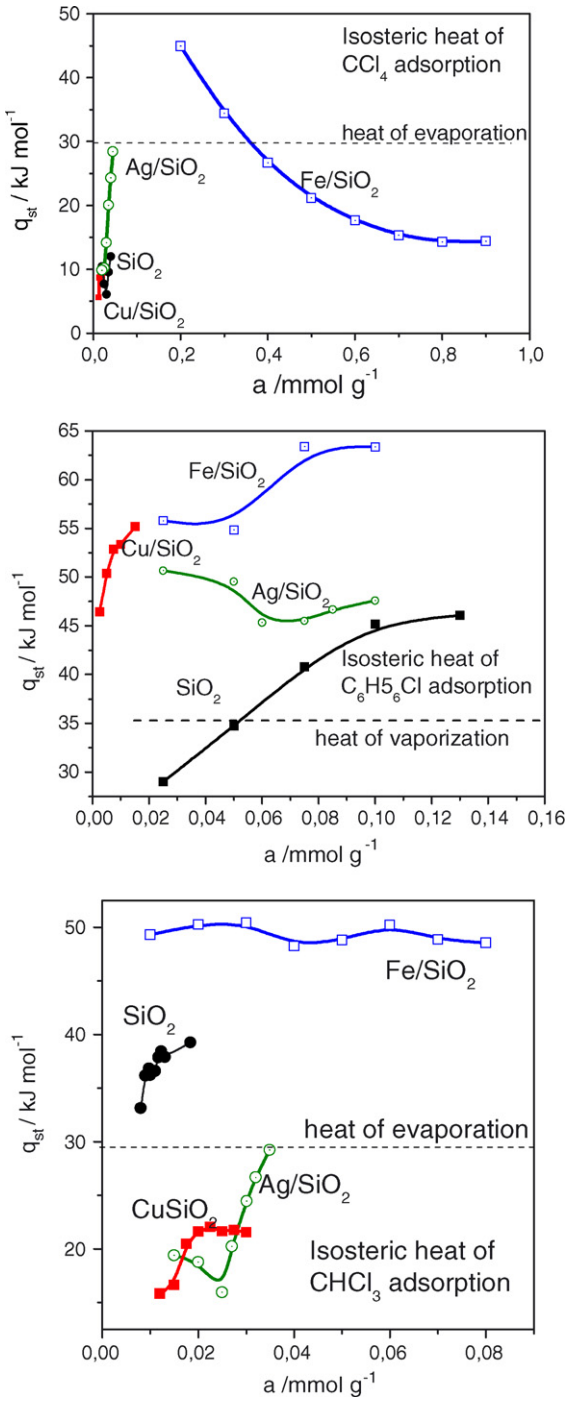


**Fig. 9.** Variation of the isosteric heat of adsorption ($-q_{st}$, kJ mol$^{-1}$) of $C_6H_5Cl$, $CHCl_3$, and $CCl_4$ with adsorbate loading on undoped and metal-doped $SiO_2$ sol–gel substrates.

the following decreasing order:

$C_6H_5Cl$ : $Fe/SiO_2 > Cu/SiO_2 > Ag/SiO_2 > SiO_2$;

$CHCl_3$: $Fe/SiO_2 > SiO_2 > Ag/SiO_2 > Cu/SiO_2$;

$CCl_4$: $Fe/SiO_2 > Ag/SiO_2 > SiO_2 > Cu/SiO_2$

There exists an almost total concordance between the tendencies of the $q_{st}$ and $-\Delta U_0$ values for each adsorptive. The adsorption heats of chlorinated compounds on the $SiO_2$, $Ag/SiO_2$, $Cu/SiO_2$, and $Fe/SiO_2$ materials increase (not all, but in general) with the surface coverage thus indicating that the gas-solid adhesive interactions prevail at low pressures while the adsorbate–adsorbate cohesive interactions start to dominate at higher pressures. Part of the solid–adsorbate interactions can be associated to the attractive forces (i.e. weak hydrogen bonds) existing between the Cl atoms of the chlorinated compounds and the silanol groups (Si—OH) attached to the silica surface. It is observed that the surfaces of the metal-doped $SiO_2$ substrates present, in general, smaller energy heterogeneities than those associated to the material made of pure silica, since it is known that in homogeneous surfaces $q_{st}$ steadily decreases with increasing surface coverage [30].

## 4. Conclusions

Based on the texture analysis as evaluated from $N_2$ adsorption at 76 K, it can be concluded that the sol–gel silica adsorbents represent different valuable options for the effective capture of hazardous chlorinated compounds. The parent $SiO_2$ sol–gel adsorbent is basically mesoporous and depicts the largest total pore volume of all; nevertheless, the inclusion of metallic dopants within the amorphous silica structure usually involves stronger attractive interactions (i.e. larger $q_{st}$ and $-\Delta U_0$ values) with the adsorbate molecules thus increasing the trapping efficiency with respect to that of the undoped silica material.

Despite their lower pore volumes (if compared to the $SiO_2$ material), the $Fe/SiO_2$, $Ag/SiO_2$ and $SiO_2$ substrates represent useful micropore–mesopore adsorbent options for the capture of chlorinated vapors, even at relatively high temperatures. On the other hand, the $Cu/SiO_2$ adsorbent is mostly a mesoporous solid. The $N_2$ desorption isotherm of this sample indicates the presence of some cavities surrounded by narrow necks. The coexistence of micropores and mesopores in the $Fe/SiO_2$ and $Ag/SiO_2$ specimens offers an additional advantage: a rapid transport of molecules through the mesopore channels and a strong retention of the adsorbate within the micropores. The $SiO_2$ material is devoid of this micropore-mesopore coexistence.

The adsorption isotherms obtained experimentally for the silica substrates ($SiO_2$, $Ag/SiO_2$, $Cu/SiO_2$ and $Fe/SiO_2$) are adjusted to the adsorption pattern predicted by the Freundlich equation. The isosteric heats of adsorption in the silica materials are associated to the interactions existing between the molecules of the chlorinated compounds and the silanol groups (Si—OH) linked to the surfaces of silica. The adsorbent surface when doped with metals presents smaller energy heterogeneity if compared to that of the pure silica adsorbent.

## Acknowledgment

This research was supported by funds provided by the Consejo Nacional de Ciencia y Tecnología de Mexico (CONACYT) through grant 47631-F.

## References

[1] http://www.epa.gov/superfund/policy/cercla.htm Comprehensive Environmental Response, Compensation, and Liability Act (CERCLA), U.S. Environmental Protection Agency, 2005.
[2] F. Stoeckli, A. Lavanchy, D. Hugi-Cleary, Dubinin's theory: a versatile tool in adsorption science, in: F.A. Meunier (Ed.), In Fundamentals of Adsorption VI, Elsevier, Amsterdam, 1998, pp. 75–80.
[3] R.A. Roberts, K.S.W. Sing, V. Tripathi, Adsorption of nitrogen and neopentane vapor by microporous carbons, Langmuir 3 (1987) 331–335.
[4] A. Matsumoto, J. Zhao, K. Tsutsumi, Adsorption behavior of hydrocarbons on slit-shaped micropores, Langmuir 13 (1997) 496–501.
[5] F. Kooli, Y. Kiyozumi, V. Rives, F. Mizukami, Langmuir 18 (2002) 4103–4110.
[6] M.J. Remy, G.A. Poncelet, New approach to the determination of the external surface and micropore volume of zeolites from the nitrogen adsorption isotherm at 77 K, J. Phys. Chem. 99 (1995) 773–779.
[7] Y. Lu, G. Cao, R.P. Kale, S. Prabakar, G.P. Lopez, C.J. Brinker, Microporous silica prepared by organic templating: relationship between the molecular template and pore structure, Chem. Matter 11 (1999) 1223–1229.
[8] C.J. Brinker, S. Wallace, N.K. Raman, R. Sehgal, J. Samuel, S.M. Contakes, Sol–gel processing of amorphous nanoporous silicas, access, in: T.J. Pinnavaia, M.F. Thorpe (Eds.), Nanoporous Material, Plenum Press, New York, 1995, pp. 123–159.
[9] P.A. Gordon, E.D. Glandt, Alkane adsorption on microporous silica gel, in: F.A. Meunier (Ed.), Fundamentals of Adsorption VI, Elsevier, Amsterdam, 1998, pp. 105–110.
[10] J. Limpo, M.C. Bautista, J. Rubio, J.L. Oteo, Effect of heating on surface area and pore size distribution of monolithyc silica gels, in: J. Rouquerol, F. Rodriguez-Reinoso, K.S.W. Sing, K.K. Unger (Eds.), Characterization of Porous Solids III, Elsevier, Amsterdam, 1994, pp. 429–437.
[11] N.K. Raman, M.T. Anderson, C.J. Brinker, Template-based approaches to the preparation of amorphous, nanoporous silicas, Chem. Mater. 8 (1996) 1682–1701.
[12] M.A. Hernández, A. Velasco, F. Rojas, M. Asomoza, S. Solís, V.H. Lara, M.A. Salgado, R. Portillo, Alkane adsorption on microporous $SiO_2$ substrata. 1. Textural characterization and equilibrium, Energy Fuels 17 (2003) 262–270.
[13] M.A. Hernández, A. Velasco, F. Rojas, M. Asomoza, S. Solís, V.H. Lara, M.A. Salgado, R. Portillo, Adsorption of benzene, toluene, and *p*-xylene on microporous $SiO_2$, Ind. Eng. Chem. Res. 43 (2004) 1779–1787.
[14] D.L. Meixner, A.G. Gilicinski, P.N. Dyer, "Figure/ground" study of colloidal silica nanoparticles and corresponding microporous xerogels, Langmuir 14 (1998) 3202–3209.
[15] K.S.W. Sing, R.T. Williams, The use of molecular probes for the characterization of nanoporous adsorbents, Part. Part. Syst. Charact. 21 (2004) 71–79.
[16] S.J. Gregg, K.S.W. Sing, Adsorption, Surface Area, and Porosity, Academic Press, London, 1982.
[17] P.I. Ravikovitch, S.C.O. Domhnaill, A.V. Neimark, F. Schueth, K.K. Unger, Capillary hysteresis in nanopores: theoretical and experimental studies of nitrogen adsorption on MCM-41, Langmuir 11 (1995) 4765–4772.
[18] P.I. Ravikovitch, A.V. Neimark, Characterization of micro- and mesoporosity in SBA-15 materials from adsorption data by the NLDFT method, J. Phys. Chem. B 105 (2001) 6817–6823.
[19] V.R. Choudhary, K. Mantri, Adsorption of aromatic hydrocarbons on highly siliceous MCM-41, Langmuir 16 (2000) 7031–7037.
[20] H. Pan, J.A. Ritter, P.B. Balbuena, Examination of the approximations used in determining the isosteric heat of adsorption from the Clausius–Clapeyron equation, Langmuir 14 (1998) 6323–6327.
[21] P. Basu, T.H. Ballinger, J.T. Yates, Wide temperature range IR spectroscopy cell for studies of adsorption and desorption on high area solids, Rev. Sci. Instrum. 59 (1988) 1321–1327.
[22] T.-G. Kim, Y. Woon Kim, J. Soon Kim, B. Park, Silver-nanoparticle dispersion from the consolidation of Ag-attached silica colloid, J. Mater. Res. 19 (2004) 1400–1407.
[23] P.I. Ravikovitch, D. Wei, W.T. Chueh, G.L. Haller, A.V. Neimark, Evaluation of pore structure parameters of MCM-41 catalyst supports and catalysts by means of nitrogen and argon adsorption, J. Phys. Chem. B 101 (1997) 3671–3679.
[24] L.C. Graton, H.J. Fraser, Systematic packing of spheres with particular relation to porosity and permeability, J. Geol. 43 (1935) 785–909.
[25] D.H. Everett, Manual of symbols and terminology for physicochemical quantities and units. Appendix II: definitions, terminology and symbols in colloid and surface chemistry, Pure Appl. Chem. 31 (1972) 577–638.
[26] A.C. Pierre, G.M. Pajonk, Chemistry of aerogels and their applications, Chem. Rev. 102 (2002) 4243–4266.
[27] L. Sarkisov, P.A. Monson, Modeling of adsorption and desorption in pores of simple geometry using molecular dynamics, Langmuir 17 (2001) 7600–7604.
[28] K. Kaneko, in: W. Rudzinski, W. Steele, G. Zgrablich (Eds.), Heterogeneous Surface Structures of Adsorbents. In Equilibrium and Dynamics of Gas Adsorption on Heterogeneous Solid Surfaces, Elsevier, Amsterdam, The Netherlands, 1994.
[29] K.S.W. Sing, D.H. Everett, R.A.W. Haul, L. Moscou, R. Pierrotti, J. Rouquerol, T. Siemienieswka, Reporting physisorption data for gas/solid systems, Pure Appl. Chem. 57 (1985) 603–619.
[30] F. Rouquerol, J. Rouquerol, K.S.W. Sing, Adsorption by Powders and Porous Solids, Academic Press, San Diego, 1999.